Available online at www.sciencedirect.com
ScienceDirect
Materials Research Bulletin 43 (2008) 1528–1538
Materials Research Bulletin
www.elsevier.com/locate/matresbu

Microwave-hydrothermal synthesis of nanostructured Na-birnessites and phase transformation by arsenic(III) oxidation

Anderson Dias [a,*], Rodrigo G. Sá [b], Matheus C. Spitale [b], Maycon Athayde [b], Virgínia S.T. Ciminelli [b]

[a] *Departamento de Química, Universidade Federal de Ouro Preto, 35400-000 Ouro Preto, MG, Brazil*
[b] *DEMET, UFMG, Rua Espírito Santo 35, Sala 206, 30160-030 Belo Horizonte, MG, Brazil*

Received 3 September 2006; received in revised form 9 April 2007; accepted 3 June 2007
Available online 9 June 2007

Abstract

Microwave-hydrothermal synthesis was employed to produce Na-birnessites. Crystalline, single-phase materials were obtained at temperatures as low as 120 °C and times as short as 1 min. X-ray diffraction and Raman spectroscopy were used to characterize the structural features of the nanostructured powders. Birnessites possessed a monoclinic structure in space group *C*2/*m* with nine Raman-active bands, all of which were observed for the first time due to optimized acquisition of the spectroscopic data. The highly reactive materials produced were submitted to sorption experiments with As(III). An oxidative precipitation occurred with the production of Mn(II) arsenate at higher arsenic concentrations. In addition, the formation of hausmannite (Mn_3O_4) was confirmed by X-ray diffraction and Raman analyses of the reacted solid phase. The observed 14 Raman-active modes were adjusted according to the tetragonal $I4_1/amd$ space group for hausmannite. An additional band related to the breathing mode of the arsenate was observed, leading to the conclusion that adsorption onto hausmannite takes place in addition to the oxidative precipitation of manganese arsenate.

Keywords: A. Oxides; B. Chemical synthesis; C. Raman spectroscopy

1. Introduction

Manganese oxides with layered structures are known as birnessites in analogy to the mineral birnessite, the most common member of the manganate family (δ-MnO_2). These materials are frequently found in diverse geological environments such as soils [1], marine manganese nodules [2,3], and Mn-rich ore deposits [4]. Also, they exhibit interesting surface-charge [5], cation-exchange [6], and redox properties, which make them highly reactive with respect to sorption phenomena [7]. Birnessites possess a layered structure in which metal ions and water molecules are located in the space between layers of edge-sharing MnO_6 octahedra. These materials can be prepared by a variety of routes and their properties are directly influenced by the processing parameters [8]. Brock et al. [8] discuss the redox reactions between permanganate and Mn(II) involved during precipitation to manganese oxides. In these processes, a mixture of

* Corresponding author. Tel.: +55 31 35591707.
E-mail address: anderson_dias@iceb.ufop.br (A. Dias).

0025-5408/$ – see front matter © 2007 Elsevier Ltd. All rights reserved.
doi:10.1016/j.materresbull.2007.06.019

manganese species dominated by birnessites and hausmannite (Mn_3O_4) is frequently produced. The birnessites can also incorporate cations (typically alkali or alkaline earth metal ions) and hydronium ions between the layers to balance the negative charge on the sheets [9]. Hydrothermal synthesis is another method that has been extensively employed to produce a variety of manganese-based porous structures, including birnessites [10] and todorokites [11]. Parameters of pH, temperature, type of anion (acetate, chloride, nitrate, sulfate), MnO_4^-/Mn^{2+} ratio, and type of other cations like Mg^{2+} were investigated for their effect on the crystallinity and morphology of the precipitates [10,11].

Recently, the combination of hydrothermal processing and microwave energy enabled significant savings in time and energy costs due to shorter processing times and more homogeneous products [12]. New materials and improved microstructures also have been reported in different systems like phosphates [13], zeolites [14] and electroceramics [15]. In microwave heating, the material absorbs microwaves (interaction with the dipole moment of water) and converts this electromagnetic energy to heat. In contrast with conventional autoclave heating, microwave energy heats materials more evenly, with little or no temperature gradients from the surface to the inside [12]. In this work, the microwave-hydrothermal synthesis of birnessites is reported for the first time. Nanostructured and highly reactive materials were produced in very short times and moderate temperatures. The results led us to explore arsenic(III) oxidation and the sorption capacity of the obtained birnessites. Manganese oxides are currently used by industry in the treatment of water, e.g., using manganese greensand filtration systems [16]. Today, many commercially available manganese-based oxides are considered by the U.S. Environmental Protection Agency as oxidizing and adsorptive media in industrial applications [17]. In the present work, X-ray diffraction (XRD) and Raman spectroscopy were employed to evaluate the structural features of manganese oxides before and after oxidation/adsorption experiments. Raman scattering is a technique very sensitive to short-range order and highly applicable to amorphous compounds [18]. It yields a more complete and reliable structural description than XRD of the manganese oxides studied here, where some crystalline disorder may be expected. In this study, it was possible for the first time to obtain a complete Raman spectrum of Na-birnessites obtained after careful Raman analyses, which allowed the fulfillment of the theoretical predictions in the experimental data.

2. Experimental

$MnCl_2{\cdot}4H_2O$ (>99%), NaOH (>99%) and $KMnO_4$ (>97%) were employed as starting materials. The reagents were weighed and dissolved in deionized water (18.2 MΩ cm). Manganese chloride was mixed with NaOH to produce manganese hydroxide, followed by the addition of potassium permanganate while stirring at pH 12. Microwave-assisted hydrothermal experiments were performed using a Milestone MLS-1200 MEGA microwave digestion system (2.45 GHz). This system operates at a maximum power of 1000 W, and power can be varied from 0 to 100% controlled by both pressure (autogenous pressure) and temperature. The system was programmed to work at various power levels (400–1000 W) up to the processing temperature (120–180 °C) and maintained there for times between 1 and 60 min.

The precipitates were washed with water and centrifuged to remove all the NaCl formed and dried overnight at 80 °C. Crystalline phases were identified by XRD in a Philips PW1710 diffractometer with Cu Kα radiation (40 kV, 30 mA) and a graphite monochromator, analyzing from 10° to 100° 2θ at a speed of 0.02° 2θ/s. Scanning electron microscopy and energy-dispersive spectrometry (Thermo Noran) were carried out in a Jeol-6360 LV instrument (15 kV). Nitrogen adsorption for determination of the surface area was accomplished in equipment from Quantachrome (NOVA-1000) in samples degassed at 150 °C for 1 h.

Micro-Raman scattering spectra were recorded using a *Jobin-Yvon* LABRAM-HR 800 spectrometer, equipped with 600 and 1800 grooves/mm diffraction grating, a liquid-N_2-cooled CCD detector and a confocal microscope (100× objective). The experimental resolution was better than 1 cm^{-1}. After deconvolution, the ultimate resolution was 0.2 cm^{-1}. The measurements were carried out in back-scattering geometry at room temperature, using the 632.8 nm line of a helium–neon ion laser (maximum laser power of 12.5 mW) as excitation source. A holographic notch filter was used to stray light rejection (Rayleigh scattered light). Repeated analyses were done beginning at very lower laser powers, in order to avoid phase transformation, and then incrementally increasing the power after each set of analyses. In this way, untouched surfaces were studied for determination of the better signal/noise ratio with no possibility of creation of new phases through laser heating of the samples in the presence of oxygen (air). The best condition for analyses was found at 0.125 mW of laser power through 100 accumulations of 300 s each.

Adsorption experiments were carried out in closed flasks containing different amounts of Na-birnessite and As(III) solutions. The experiments were conducted in a shaker (sealed flasks) with controlled temperature (25 °C) and

agitation for 24 h. Arsenic solutions were prepared by using $NaAsO_2$ (>98%) in deionized water (1–800 mg L^{-1}). The ionic strength was adjusted with NaCl to μ = 0.15 mol L^{-1} and pH 8 (NaOH). Chemical analyses were carried out by atomic absorption spectrometry (Perkin-Elmer Analyst 300) and inductively coupled plasma mass-spectrometry ICP-MS (Perkin-Elmer ELAN 9000). Additional experiments with As(V) were conducted in similar conditions in order to analyze the adsorption process itself, which help us to examine the non-oxidative behavior of our manganese oxides.

3. Results and discussion

3.1. Microwave-hydrothermal synthesis

The results of XRD analyses showed that all samples produced by microwave-hydrothermal synthesis were impurity-free, single-phase materials. Fig. 1 presents a typical diffractogram for the sample produced after 1 min at 120 °C. Peaks of Na-birnessite ($Na_{0.55}Mn_2O_4{\cdot}1.5H_2O$) were observed and could be indexed by the ICDD card #43-1456. At low 2θ angles (around 12.4°), the predominant peak is assigned to the basal spacing of the lamellar structure (7.15 Å). The preferential orientation observed by the high intensity of the (0 0 1) Bragg line would be due to the alignment of the MnO_6 layers (basal planes) parallel to the surface of the sample during the XRD acquisition. The materials present a defect structure [19] and display 0 0 *l* reflections and additional broad peaks having 1 0 0 and 1 1 0 indices with $d_{1\,0\,0}$ = 2.43 Å and $d_{1\,1\,0}$ = 1.42 Å. Holland and Walker [19] define this defect structure as the result of the few constraints on the spatial relationship between adjacent layers. Based on the indices assumed for the microwave-hydrothermal birnessites, a monoclinic structure with space group *C*2/*m* and *Z* = 1 is expected. However, another possible structure was found in the ICDD card #23-1046 for a classical birnessite structure ($Na_4Mn_{14}O_{27}{\cdot}9H_2O$), which possesses orthorhombic symmetry and *Z* = 3, as also verified by Giovanoli and co-worker [20]. Although indexing of the microwave-hydrothermal birnessites is similar for both the monoclinic and orthorhombic systems, there is a tendency in the literature to assume the monoclinic structure for these materials, especially after the development of advanced microscopic and spectroscopic techniques [21]. Hexagonal (H-birnessite) [21] and triclinic [22] structures also have been reported under particular conditions.

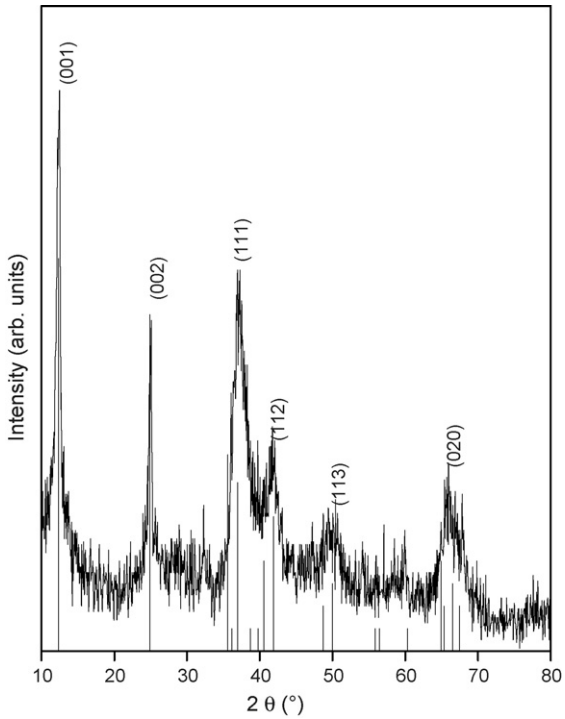

Fig. 1. XRD for the birnessite produced by microwave-hydrothermal synthesis at 120 °C for 1 min. The main Bragg lines are indexed in the figure according to the ICDD card #43-1456 (vertical lines).

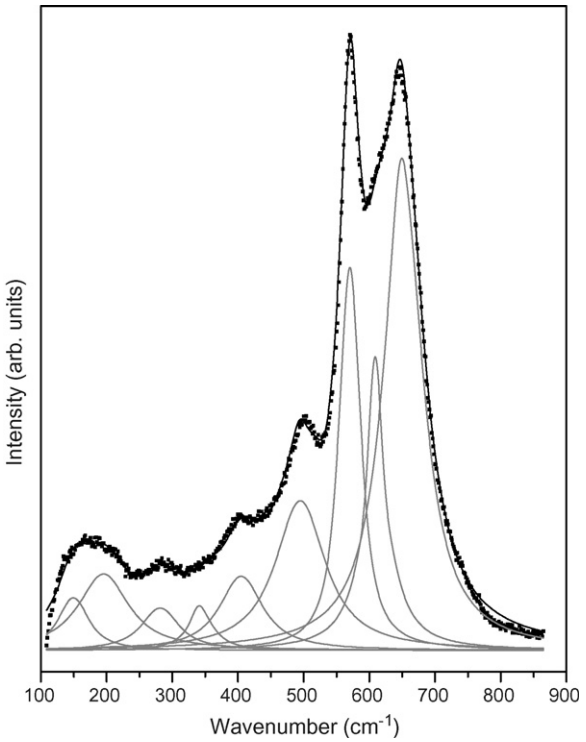

Fig. 2. Raman spectrum for the microwave-hydrothermal birnessite produced after 1 min at 120 °C. Experimental data are in solid squares and solid lines represent deconvolution by a sum of Lorentzian lines.

In view of that uncertainty in symmetry, Raman scattering was employed as a convenient and powerful local probe to determine the structure of the microwave-hydrothermal birnessites. Fig. 2 presents the experimental Raman data (solid squares) for the samples synthesized after 1 min at 120 °C. According to Julien et al. [23], a typical feature of the vibrational response of birnessites is their low Raman activity or efficiency. These authors report that the structural complexities of the birnessites require a careful analysis due to the phase instabilities frequently observed under the laser beam. Julien et al. [23] showed that most of the manganese oxides submitted to Raman analyses are changed to bixbyite (Mn_2O_3). Other authors documented the formation of spinel zones at the laser impact point [24]. In the present work, good spectra were obtained by optimizing the experimental conditions. In order to prevent phase transformation during analysis, increasing laser powers were tested at the sample surface. The final Raman data were collected by using a laser power of 0.125 mW through 100 accumulations of 300 s each. Thus, for the first time, it was possible to observe a complete spectrum of Na-birnessites, which allows us to study the structural features of these materials in more detail. As can be seen in Fig. 2, high-wavenumber bands dominate the spectrum, whereas bands in the low-frequency region have relatively low intensity. A minimum of seven bands is clearly observed, and the exact number of vibrational modes was obtained after deconvolution by a sum of Lorentzian lines. According to group theoretical calculation [25], the space groups associated with the orthorhombic, triclinic or hexagonal birnessite structures predict a number of Raman-active bands much greater than that observed in Fig. 2. For the monoclinic $C2/m$ space group with $Z = 1$, use of the site-group method of Rousseau et al. [25], produces the following irreducible representations:

$$\Gamma = 3A_g \oplus 4A_u \oplus 6B_g \oplus 8B_u. \quad (1)$$

According to the above equation, there are 9 Raman-active modes ($3A_g$ and $6B_g$) and 12 infrared-active modes ($4A_u$ and $8B_u$) for this group. Fig. 2 shows the experimental spectrum after deconvolution (solid lines) with nine Lorentzian curves, which led us to believe that the microwave-hydrothermal birnessites belong to the monoclinic $C2/m$ space group.

Table 1 shows the Raman parameters, frequency and full width at half-maximum, obtained from the deconvolution of the experimental data in Fig. 2. The results showed no discrepancies between factor-group analysis and Raman data,

Table 1
Raman fitting parameters for the birnessite produced after 1 min at 120 °C

Band	Position (cm^{-1})	FWHM (cm^{-1})
1	149.7	50.2
2	195.6	89.4
3	281.7	64.0
4	343.5	44.6
5	404.9	75.1
6	495.0	87.6
7	570.4	32.1
8	610.2	52.7
9	651.3	68.9

FWHM is the full width at half-maximum.

contrary to the report by Julien et al. [23], who observed a maximum of six bands in their samples. This fact is probably due to the long acquisition time and large number of accumulations in the present work. The complete assignment of all bands is difficult because of the lack of single crystals or selection rules that allow experiments employing polarization for separation of the vibrational modes. Plausible assignments can be made for a few Raman bands. The mode centered at 651.3 cm^{-1} can be assigned to the symmetric stretching vibration ν_2 (Mn–O) of MnO_6 groups, or the A_{1g} symmetric mode [23,26]. The band located at 570.4 cm^{-1} is usually attributed to the ν_3 (Mn–O) stretching vibration in the basal plane of the MnO_6 sheets [23,26]. The other bands could be related to the stretching modes of NaO_6 groups (below 300 cm^{-1}) and the NaO_4 tetrahedron (300–500 cm^{-1}), according to the structural considerations of Le Goff et al. [27] and Julien et al. [23,26]. Na and K ions are assumed to be positioned in trigonal prismatic sites of the interlayer space [26,27], with an interplanar spacing of $d = 7.15$ Å measured in the present samples, corresponding to two adjacent nonsuperimposed MnO_6 octahedral sheets.

3.2. Arsenic(III) oxidation and adsorption

After careful structural analysis of the microwave-hydrothermal birnessites, the morphological features were evaluated in order to verify their response to oxidation and adsorption experiments. Specific surface areas were measured by nitrogen adsorption for all samples and the values were around 45 m^2/g, which correspond to particle sizes on the order of 35 nm. These results agree reasonably well with the 25 nm calculated based on XRD (full width at half-maximum and the Debye–Scherrer equation). Also, nanostructured birnessites were observed by scanning electron microscopy to have soft agglomeration, as expected in hydrothermal synthesized powders [15]. These highly reactive materials produced by microwave-hydrothermal synthesis were investigated in terms of their ability to oxidize and adsorb As(III). This chemical species was chosen because of its relevance to environmental studies and the well-known adsorption characteristics in manganese-based oxides [3,7,28,29]. The toxicity, mobility, and bioavailability of arsenic in soil–water systems are highly dependent on its oxidation state and chemical speciation [28,29]. The reduced species, As(III), is much more toxic, and mobile than the oxidized species, As(V). Several investigations have focused on the immobilization of arsenic by natural and synthetic iron oxides and iron hydroxides [30]. However, few works have focused on the immobilization of arsenic by manganese oxides [29] despite the fact that these materials are known as effective oxidizers of As(III) to As(V) in natural environments and in water treatment units [16,17]. In order to decrease the levels of arsenic in water, in accordance with regulatory limits, it is important to investigate synthetic adsorbents suitable to oxidize and adsorb arsenic.

In this work, the influence of high As(III) concentration in solution on the crystalline phases after oxidation and adsorption experiments were evaluated by XRD and Raman spectroscopy. Adsorption isotherms were constructed for all microwave-hydrothermal samples, which showed maximum levels for adsorption of around 20 mg As g^{-1} birnessite. These results are rather better to those obtained by our group in adsorption experiments conducted with iron- and aluminum-based soils and oxides [30], as well as with combined Mn- and Fe-based minerals [29]. Increasing arsenic levels were observed for higher As concentration in solution, which are due to precipitation, as discussed below. In the present work, we infer that oxidation and adsorption of As were favored by the nanostructured nature of

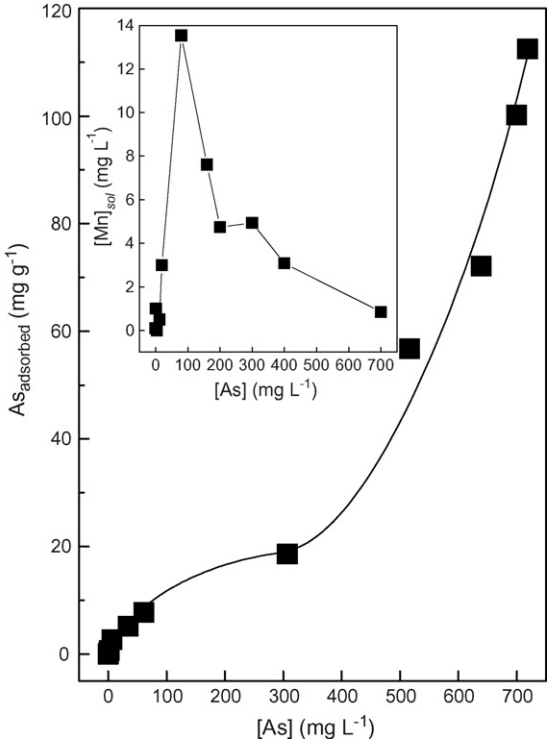

Fig. 3. Adsorption isotherm (25 °C, 24 h, ionic strength of 0.15 mol NaCl/L and pH 8) for As on the microwave-hydrothermal birnessite obtained at 120 °C, for 1 min. Inset: manganese concentration in solution (mg L^{-1}) after adsorption experiments.

the microwave-hydrothermal birnessites. Fig. 3 shows the isotherm for arsenic uptake by the birnessite produced at 120 °C, after 1 min. The accepted standard deviation was within 5%. A classical Langmuir-type curve can be observed for arsenic concentrations up to 300 mg L^{-1}. For higher As concentration in solution, increasing arsenic levels were measured in the solid phase after adsorption, i.e., typical of precipitation [31]. Also, the inset in this figure shows the manganese concentrations in solution after adsorption experiments. Measurements of dissolved manganese after oxidation showed only negligible amounts for As concentrations below 80 mg L^{-1}. At higher As concentrations in solution, manganese was released to the solution with a maximum occurring at [As] = 100 mg L^{-1}, followed by a decrease in dissolved Mn with further increase in As concentrations. Similar results were also observed by Driehaus et al. [31], who studied the oxidation of As(III) by δ-MnO_2. The authors verified a lack of manganese release at lower As concentrations and attributed this result to the high adsorption capacity of manganese oxides for soluble manganese, though precipitation was not ruled out. Many authors have discussed the possible formation and nature of this manganese arsenate precipitate; however, they provided no direct evidence. In the present work, the analysis of the solid phases was carried out in order to better understand this manganese removal.

Fig. 4 presents XRD analysis of the oxidation and adsorption experimental products as a function of dissolved arsenic concentration in solution (starting with the unreacted material) for the sample obtained at 120 °C for 1 min. It was observed that the increase in the As concentration promoted the dissolution of the birnessite, deduced by the reduction in the intensity of the (0 0 1) Bragg line at 12.4° 2Θ. We also verified the concurrent production of hausmannite, Mn_3O_4 (ICDD card #80-0382), as well as the precipitation of a manganese arsenate, $Mn_3(AsO_4)_2{\cdot}4H_2O$ (ICDD card #35-0478) in materials submitted to higher arsenic concentrations (the latter is marked with an asterisk in Fig. 4). The peaks of hausmannite coincide with those of birnessite in the region 35–40° 2Θ [32], which makes its identification difficult during the oxidative precipitation of manganese arsenate by XRD. Fig. 5 presents the intensities of the main diffraction peak for each phase as a function of arsenic concentration. For As concentration as low as 0.2 mg L^{-1}, the intensity of the (0 0 1) Bragg line of the birnessite decreased as arsenic concentration increased. The solid phase $Mn_3(AsO_4)_2{\cdot}4H_2O$ was detected after experiments with 160 mg As L^{-1} (chemical analyses showed a sudden decrease in Mn concentration in solution at this As level) and presented a maximum at 300 mg L^{-1}, as shown

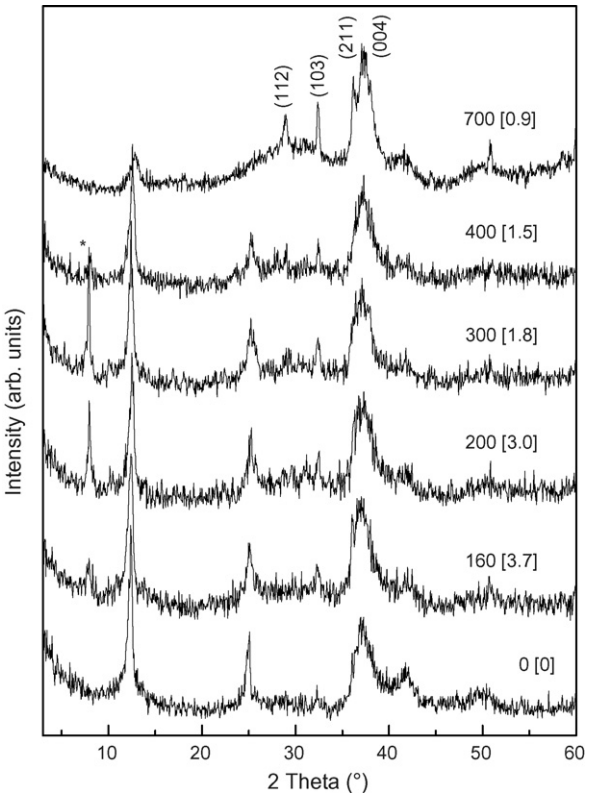

Fig. 4. XRD results for the birnessite obtained at 120 °C, for 1 min, as a function of As(III) concentration (mg L^{-1}) in solution. Manganese arsenate starts to precipitate at 160 mg As L^{-1}, as marked with an asterisk in the figure. Mn/As ratios are indicated in brackets besides As(III) concentrations. The planes (1 1 2), (1 0 3), (2 1 1), and (0 0 4) of the hausmannite are also indicated.

in Fig. 5. For As concentrations increasing up to 400 mg L^{-1}, the final pH decreased from 7.7 to 6.8. At the highest As concentration employed (700 mg L^{-1}), the main peak of the manganese arsenate had disappeared, which will be discussed further.

The results allowed the construction of a reaction scheme for the birnessite-H_3AsO_3 system. Chemically, the reactions that would occur can be interpreted as an oxidative precipitation of manganese arsenate or a reductive dissolution of birnessite besides the adsorption of arsenate ions onto hausmannite. The functional groups ◀MnO_2 and ◀Mn_H-OH presented below are considered to be the birnessite- and hausmannite-active groups available at the surface for arsenic oxidation and adsorption:

$$6{\blacktriangleleft}MnO_2 + 4H_3AsO_3 \rightarrow 2Mn_3O_4 + 4HAsO_4^{2-} + 8H^+; \quad (2a)$$

$$Mn_3O_4 + H_3AsO_3 + 4H^+ \rightarrow 3Mn^{2+} + HAsO_4^{2-} + 3H_2O; \quad (2b)$$

$${\blacktriangleleft}MnO_2 + H_3AsO_3 \rightarrow Mn^{2+} + HAsO_4^{2-} + H_2O; \quad (2c)$$

$$3Mn^{2+} + 2HAsO_4^{2-} \rightarrow Mn_3(AsO_4)_2 + 2H^+; \quad (2d)$$

$${\blacktriangleleft}Mn_H\text{-}[OH] + HAsO_4^{2-} + 2H^+ \rightarrow Mn_H\text{-}[AsO_4] + 2H_2O. \quad (2e)$$

The schematic reactions listed above demonstrate that the birnessites were fully consumed during the oxidative precipitation, producing hausmannite (Eq. (2a)), arsenate ions (Eq. (2a)) and soluble manganese (Eq. (2c)). The first reaction generates H^+ and pH must fall. However, hausmannite could also oxidize As(III) ions producing more soluble

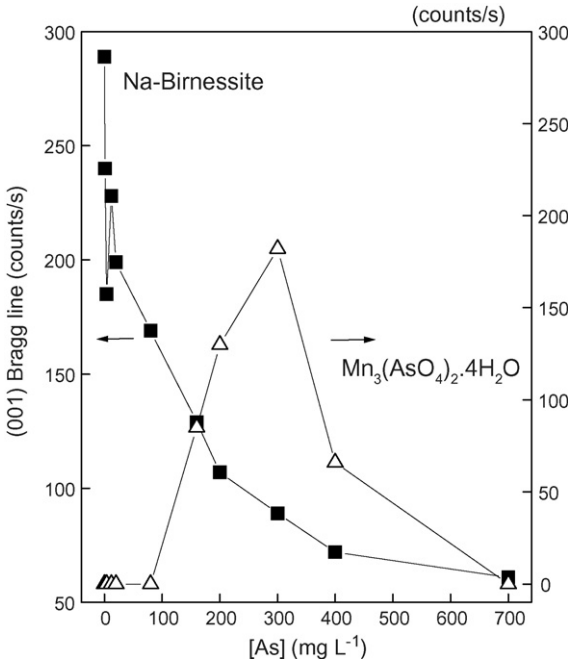

Fig. 5. XRD intensities for the (0 0 1) Bragg line of birnessite (left side) and for a manganese arsenate (right side) as a function of the dissolved arsenic concentration.

manganese and $HAsO_4^{2-}$ (Eq. (2b)). The reaction consumes partially the H^+ produced in the initial step, which avoids an accentuated decrease in the pH value. Finally, Mn(II) reacts with arsenate to precipitate the solid phase $Mn_3(AsO_4)_2{\cdot}4H_2O$ (Eq. (2d)). Then, the adsorption of arsenate ions onto hausmannite occurs, which also prevents the decrease in the pH value (Eq. (2e)). The overall result indicates that both hausmannite and manganese arsenate are produced, together with $HAsO_4^{2-}$ ions that adsorb onto hausmannite. Previous works [33–35] showed good evidence that a product formed by Mn(III) ions should appear as an intermediate product after reductive dissolution of birnessite. Nesbitt et al. [33] presented the best results in this subject by using X-ray photoelectron spectroscopy (XPS). The authors showed that a Mn(III)-oxyhydroxide was obtained as a metastable phase, which is reduced to Mn(II) afterwards, as also verified in the presented work. Many authors revisited these reactions but no work has observed the presence of hausmannite as final product [34,35]. In this respect, the identification of hausmannite and the confirmation of the presence of the solid phase $Mn_3(AsO_4)_2{\cdot}4H_2O$ by XRD can be considered original contributions of this work. Concerning the adsorption of arsenate ions onto hausmannite, it is believed that the latter's surface becomes progressively hydroxylated and hydrated as reaction proceeds, in agreement with the results of Manning et al. [35], which concluded that an inner-sphere bidentate binuclear complex is formed with an As–Mn interatomic distance of 3.22 Å.

The reactions reported in the last paragraph together with the absence of the XRD peak for manganese arsenate for As concentration of 700 mg L^{-1} introduce new approaches to understand the mechanisms of birnessite dissolution and also raise an important question: why does the quantity of solid phase $Mn_3(AsO_4)_2{\cdot}4H_2O$ attain a maximum and then suddenly disappear? First, it is important to note that Mn/As ratios of 1.5 and 1.0 are required to produce hausmannite (Eq. (2a)) and Mn(II) (Eq. (2c)), respectively. In the beginning of the birnessite dissolution (or lower As concentrations), the molar Mn/As ratio is much higher than 1.5 (see Fig. 4). Under these conditions, hausmannite would be produced, which is the main source of Mn(II) through Eq. (2b) (the final pH would not be altered at all). Consequently, $Mn_3(AsO_4)_2{\cdot}4H_2O$ could be obtained, since the amount of Mn(II) is sufficiently high ($Mn^{2+}/AsO_4 = 3$ in Eq. (2b)) to produce this solid phase (higher thermodynamic driving force). This reaction generates H^+ and the pH falls, Eq. (2d), as verified experimentally. In higher As concentrations, another reaction (Eq. (2c)) starts to dominate (the molar ratio birnessite:H_3AsO_3 is 1:1), i.e., the source of Mn(II) is the birnessite itself. In the present work, the Mn/As ratio attained a minimum at 700 mg As L^{-1}: 0.9 (see Fig. 4). Hausmannite stops being reduced to produce Mn(II) ions and, consequently, manganese arsenate does not meet the thermodynamic requirements to precipitate (the driving

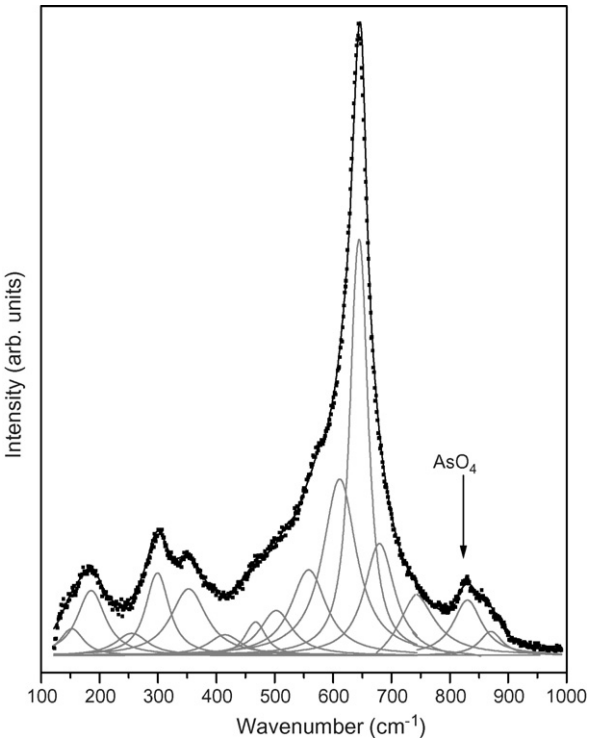

Fig. 6. Raman spectrum obtained for the microwave-hydrothermal birnessite (120 °C, 1 min) after undergoing oxidative precipitation. Experimental data are shown as solid squares, whereas solid lines represent deconvolution by a sum of Lorentzian curves. The phase is shown to be hausmannite. Arsenate breathing mode is also indicated in the figure.

force decreases considerably). The adsorption reaction between the arsenate species and hausmannite (Eq. (2e)) is a schematic representation of what happens during dissolution of the birnessites.

Finally, Raman spectroscopy was applied to characterize the solid phase after contact with the highest As concentration (Mn/As = 0.9, top curve in Fig. 4). Fig. 6 presents the spectrum for the sample after oxidative precipitation (experimental data in solid squares). In general, an increase in the number of bands was observed in comparison with the original birnessite (Fig. 2). According to the schematic reactions displayed in Eqs. (2a)–(2e) and the XRD results, hausmannite is the only expected solid phase to be identified by Raman spectroscopy (Fig. 4). For this compound, factor-group analysis was carried out considering a distorted spinel structure [36] with space group $I4_1/amd$ ($Z = 4$). Applying the method of Rousseau et al. [25], the following irreducible representation was obtained after subtraction of the acoustic modes:

$$\Gamma = 2A_{1g} \oplus 4A_u \oplus 2B_{1g} \oplus 4B_{2g} \oplus 6E_g \oplus 6E_u. \quad (3)$$

This result shows that 14 Raman-active and 10 infrared-active modes are expected. Fig. 6 shows the experimental spectrum after deconvolution with a sum of 15 Lorentzian curves. Table 2 presents the fitting parameters for this sample. The spectrum of Mn_3O_4 is characterized by a very sharp band at 644 cm^{-1} and is characteristic of the mineral hausmannite and other spinel structures, like magnetite [32,36]. It can be assigned to the A_{1g} mode, which corresponds to the Mn–O breathing vibration of divalent manganese ions in tetrahedral coordination [23]. In the vibrational modes of species A_{1g}, only motions of the oxygen atoms are involved. It is assumed that bonding and repulsion effects (covalence of Mn–O bonds) interfere in the breathing mode of the tetrahedral MnO_6 units [23]. In the present work, we believe that 14 Raman-active modes observed in Fig. 6 could be due to the hausmannite, while the 15th band could be associated to the presence of arsenate at 830 cm^{-1} (AsO_4 breathing mode) [28]. This result shows that the arsenic was oxidized from the trivalent state to pentavalent state and is adsorbed by hausmannite, as also verified by Deschamps et al. [29] in natural iron–manganese-based oxides. Additional experiments with As(V) help us to confirm these results, since for this species a non-oxidative process occur (Raman spectra showed only the arsenate band at 830 cm^{-1}), not showed in the present work.

Table 2
Raman fitting parameters for the birnessite produced at 120 °C, for 1 min, after oxidative precipitation and adsorption experiments

Band	Position (cm^{-1})	FWHM (cm^{-1})
1	152.4	43.8
2	185.7	54.2
3	255.0	63.8
4	299.1	43.6
5	352.5	70.0
6	414.8	65.4
7	467.1	37.1
8	502.6	63.9
9	558.1	69.4
10	611.2	65.9
11	644.4	30.6
12	679.3	58.4
13	739.5	81.1
14	830.1	58.8
15	870.4	46.0

4. Conclusions

Crystalline, single-phase birnessites were produced for the first time by microwave-hydrothermal synthesis using moderate temperatures and short reaction times. Nanostructured powders with high reactivity with respect to sorption phenomena were obtained and submitted to experiments with trivalent arsenic. Structural analysis of the materials before and after sorption was carried out by XRD and Raman spectroscopy. Birnessites showed a monoclinic *C*2/*m* space group with nine Raman-active modes, which were deconvoluted by a sum of Lorentzian lines. This result was only possible because of the unusually good signal/noise ratio of the Raman data. After contact with As(III) solutions, birnessites (Mn^{4+}) were converted to hausmannite (Mn^{2+} and Mn^{3+}) through the oxidation of As^{3+} to As^{5+}. Raman analysis of the solid phase after the oxidative precipitation showed a typical spectrum of tetragonal $I4_1/amd$ hausmannite with 14 Raman–active modes together with an additional band related to the AsO_4 breathing mode. The presence of this band demonstrates that Mn_3O_4 can adsorb the arsenate ions. For higher arsenic concentrations, the precipitation of manganese arsenate occurred.

Acknowledgements

The authors acknowledge the financial support from MCT/CNPq, FINEP, and FAPEMIG. The present work is part of the Millennium Science Initiative: Water, A Mineral Approach.

References

[1] F.V. Chukhrov, A.I. Gorshkov, E.S. Rudnitskaya, V.V. Beresovskaya, A.V. Sivtsov, Clay Clay Miner. 28 (1980) 346.
[2] F.V. Chukhrov, A.I. Gorshkov, A.V. Sivtsov, V.V. Beresovskaya, Nature 280 (1979) 136.
[3] M.A. Marcus, A. Manceau, M. Kersten, Geochim. Cosmochim. Acta 68 (2004) 3125.
[4] J.E.P. Post, Natl. Acad. Sci. U.S.A. 96 (1999) 3447.
[5] R.M. Mckenzie, Aust. J. Soil Res. 19 (1981) 41.
[6] N.Z. Misak, E.M. Mikhail, Solvent Extr. Ion Exch. 5 (1987) 939.
[7] I.A. Katsoyiannis, A.I. Zouboulis, M. Jekel, Ind. Eng. Chem. Res. 43 (2004) 486.
[8] S.L. Brock, N. Duan, Z.R. Tian, O. Giraldo, H. Zhou, S.L. Suib, Chem. Mater. 10 (1998) 2619.
[9] R. Chen, P. Zavalij, M.S. Whittingham, Chem. Mater. 8 (1996) 1275.
[10] A.C. Gaillot, B. Lanson, V.A. Drits, Chem. Mater. 17 (2005) 2959.
[11] D.C. Golden, C.C. Chen, J.B. Dixon, Clay Clay Miner. 35 (1987) 271.
[12] D. Adam, Nature 421 (2003) 571.
[13] S.H. Jhung, J.W. Yoon, J.S. Hwang, A.K. Cheetham, J.S. Chang, Chem. Mater. 17 (2005) 4455.
[14] W.C. Conner, G. Tompsett, K.H. Lee, K.S. Yngvesson, J. Phys. Chem. B 108 (2004) 13913.
[15] A. Dias, V.S.T. Ciminelli, Chem. Mater. 15 (2003) 1344.

[16] O.S. Thirunavukkarasu, T. Viraraghavan, K.S. Subramanian, O. Chaalal, M.R. Islam, Energy Sources 27 (2005) 209.
[17] S.K. Porter, K.G. Scheckel, C.A. Impellitteri, J.A. Ryan, Crit. Rev. Environ. Sci. Technol. 34 (2004) 495.
[18] M. Frumar, Z. Polak, Z. Cernosek, J. Non-Cryst. Solids 257 (1999) 105.
[19] K.L. Holland, J.R. Walker, Clay Clay Miner. 44 (1996) 744.
[20] R.M. Cornell, R. Giovanoli, Clay Clay Miner. 36 (1988) 249.
[21] E. Silvester, A. Manceau, V.A. Drits, Am. Mineral. 82 (1997) 962.
[22] B. Lanson, V.A. Drits, Q. Feng, A. Manceau, Am. Mineral. 87 (2002) 1662.
[23] C.M. Julien, M. Massot, C. Poinsignon, Spectrochim. Acta A 60 (2004) 689.
[24] B. Ammundsen, G.R. Burns, M.S. Islam, H. Kanoh, J. Roziere, J. Phys. Chem. B 103 (1999) 5175.
[25] D.L. Rousseau, R.P. Bauman, S.P.S. Porto, J. Raman Spectrosc. 10 (1981) 253.
[26] C.M. Julien, M. Massot, R. Baddour-Hadjean, S. Franger, S. Bach, J.P. Pereira-Ramos, Solid State Ionics 159 (2003) 345.
[27] P. Le Goff, N. Baffier, S. Bach, J.P. Pereira-Ramos, J. Mater. Chem. 4 (1994) 875.
[28] S. Goldberg, C.T. Johnston, J. Colloid Interf. Sci. 234 (2001) 204.
[29] E. Deschamps, V.S.T. Ciminelli, P.G. Weidler, A.Y. Ramos, Clay Clay Miner. 51 (2003) 197.
[30] A.C.Q. Ladeira, V.S.T. Ciminelli, Water Res. 38 (2004) 2087.
[31] W. Driehaus, R. Seith, M. Jekel, Water Res. 29 (1995) 297.
[32] B. Folch, J. Larionova, Y. Guari, C. Guérin, C. Reibel, J. Solid State Chem. 178 (2005) 2368.
[33] H.W. Nesbitt, G.W. Canning, G.M. Bancroft, Geochim. Cosmochim. Acta 62 (1998) 2097.
[34] C. Tournassat, L. Charlet, D. Bosbach, A. Manceau, Environ. Sci. Technol. 36 (2002) 463.
[35] B.A. Manning, S.E. Fendorf, B. Bostick, D.L. Suarez, Environ. Sci. Technol. 36 (2002) 976.
[36] Y. Liu, Z. Liu, G. Wang, Appl. Phys. A-Mater. 76 (2003) 1117.